REPORT DOCUMENTATION PAGE

Form Approved OMB No. 0704-0188

Public reporting burden for this collection of information is estimated to average 1 hour per response, including the time for reviewing instructions, searching existing data sources, gathering and maintaining the data needed, and completing and reviewing this collection of information. Send comments regarding this burden estimate or any other aspect of this collection of information, including suggestions for reducing this burden to Department of Defense, Washington Headquarters Services, Directorate for Information Operations and Reports (0704-0188), 1215 Jefferson Davis Highway, Suite 1204, Arlington, VA 22202-4302. Respondents should be aware that notwithstanding any other provision of law, no person shall be subject to any penalty for failing to comply with a collection of information if it does not display a currently valid OMB control number. **PLEASE DO NOT RETURN YOUR FORM TO THE ABOVE ADDRESS.**

1. REPORT DATE *(DD-MM-YYYY)*	2. REPORT TYPE	3. DATES COVERED *(From - To)*
	Technical Paper	

4. TITLE AND SUBTITLE

5a. CONTRACT NUMBER
F04611-99-C-0025

5b. GRANT NUMBER

5c. PROGRAM ELEMENT NUMBER

6. AUTHOR(S)

5d. PROJECT NUMBER

5e. TASK NUMBER

5f. WORK UNIT NUMBER

7. PERFORMING ORGANIZATION NAME(S) AND ADDRESS(ES)

ERC

8. PERFORMING ORGANIZATION REPORT

9. SPONSORING / MONITORING AGENCY NAME(S) AND ADDRESS(ES)

Air Force Research Laboratory (AFMC)
AFRL/PRS
5 Pollux Drive
Edwards AFB CA 93524-7048

10. SPONSOR/MONITOR'S ACRONYM(S)

11. SPONSOR/MONITOR'S NUMBER(S)

12. DISTRIBUTION / AVAILABILITY STATEMENT

Approved for public release; distribution unlimited.

13. SUPPLEMENTARY NOTES

14. ABSTRACT

20021030 065

15. SUBJECT TERMS

16. SECURITY CLASSIFICATION OF:			17. LIMITATION OF ABSTRACT	18. NUMBER OF PAGES	19a. NAME OF RESPONSIBLE PERSON
a. REPORT	b. ABSTRACT	c. THIS PAGE			Leilani Richardson
Unclassified	Unclassified	Unclassified	A		19b. TELEPHONE NUMBER *(include area code)* (661) 275-5015

separate
4 items enclosed

MEMORANDUM FOR PR (Contractor/In-House Publication)

FROM: PROI (TI) (STINFO) 21 Jun 2000

SUBJECT: Authorization for Release of Technical Information, Control Number: **AFRL-PR-ED-TP-2000-139**
E. Antonsen, R. Burton (University of Illinois); S. Engelman (ERC); G. Spanjers (AFRL/PRRS),
"Herriott Cell Interferometer for Density Measurements in Small-Scale Length Plasmas"

36th AIAA Joint Propulsion Conference **(Statement A)**
(Huntsville, AL, 16-19 Jul 00) **(Submission Deadline: 19 Jun 00)**

1. This request has been reviewed by the Foreign Disclosure Office for: a.) appropriateness of distribution statement, b.) military/national critical technology, c.) export controls or distribution restrictions, d.) appropriateness for release to a foreign nation, and e.) technical sensitivity and/or economic sensitivity.
Comments:_____

Signature _____ Date _____

2. This request has been reviewed by the Public Affairs Office for: a.) appropriateness for public release and/or b) possible higher headquarters review.
Comments: _____

Signature _____ Date _____

3. This request has been reviewed by the STINFO for: a.) changes if approved as amended, b.) appropriateness of distribution statement, c.) military/national critical technology, d.) economic sensitivity, e.) parallel review completed if required, and f.) format and completion of meeting clearance form if required
Comments:_____

Signature _____ Date _____

4. This request has been reviewed by PR for: a.) technical accuracy, b.) appropriateness for audience, c.) appropriateness of distribution statement, d.) technical sensitivity and economic sensitivity, e.) military/ national critical technology, and f.) data rights and patentability
Comments:_____

APPROVED/APPROVED AS AMENDED/DISAPPROVED

_____

LESLIE S. PERKINS, Ph.D (Date)
Staff Scientist
Propulsion Directorate

Herriott Cell Interferometer for Density Measurements in Small-Scale Length Plasmas

Erik Antonsen*
Rodney Burton**
University of Illinois
Urbana-Champaign, IL

Scott Engelman (ERC)†
Greg Spanjers‡
AFRL Propulsion Directorate, Edwards AFB

Abstract

The introduction of a Herriott cell into a standard quadrature heterodyne interferometer is evaluated and demonstrated to increase the resolution of the system. Measurements of electron and neutral density during and after the current pulse are sought for modeling purposes for spacecraft contamination from Pulsed Plasma Thrusters. Testing is performed on the UIUC PPT-4, a coaxial electrothermal Pulsed Plasma Thruster pulsing at 20 J. Analytical and experimental analysis is conducted to determine the integrity of the phase front and the effect of multiple passes on the density measurements taken. The phase front quality is found to be acceptable for interferometric purposes and density measurements are taken for 2, 6, 14, and 18 passes in the Herriott cell. The advantage of the cell is obvious at late times when the external room vibrations induce an apparent phase shift in the same direction as neutral particles. Due to the same dependence on wavelength, 2 laser frequencies cannot be used to separate neutral and vibration contributions. The Herriott cell allows a density resolution increase linear with the number of passes that does not increase the vibrational component. Uncertainties from both vibrational sources and shot-to-shot variations of the thruster itself are investigated and characterized for this system. Due to variations in room vibrations on a day to day basis, the cell was unable to characterize the neutral density of the thruster. However, for single tests, neutral density measurements were acquired. The Herriott cell with 18 passes introduced a 9-fold increase in resolution over the standard 2-pass interferometric setup. At 200 μs for single tests at 14 and 18 passes (~20 shots averaged) neutral density at the exit plane was shown to be no more than $1*10^{16}$ cm^{-3}. Peak electron density (4 us) was shown to be $5.0*10^{15} \pm 1.1*10^{15}$ cm^{-3}.

Introduction

The attraction of Pulsed Plasma Thrusters (PPT) as a propulsion option on small satellites stems largely from its design simplicity and use of solid, non-toxic propellant. However, in the past 30 years, research has failed to produce significant improvements in the overall performance of this thruster. Part of this is due to complex physics that are not completely understood at this point. Because of late time vaporization and small ionization fraction of the total propellant used per pulse, the typical efficiency of a PPT is around 10%. In order to improve this efficiency and harness the full potential of these thrusters, it is necessary to gain a more complete understanding of the physics behind their operation and of exactly how the propellant is being consumed.

Heterodyne quadrature interferometry has been used at the Air Force Research Laboratory (AFRL) to determine electron and neutral densities during single pulses of PPTs. Unfortunately, at long timeframes room vibrations can introduce significant error reducing the resolution available to see the slower moving neutrals. The limitations placed on the measurements by extraneous room vibrations are extensive and in the case of the UIUC PPT-4 completely masked any neutral density that was present. In order to compensate for this effect, a Herriott Cell was designed to allow laser coverage over the thruster exit plane. Typically, Herriott Cells are used to cover large plasma volumes, but in this case modifications were necessary to allow for measurements within a single plane. Additionally,

abstract shows lower case as is elsewhere in paper.

*M.S. Candidate, Department of Aeronautical and Astronautical Engineering, Student Member, AIAA.
** Professor, Department of Aeronautical and Astronautical Engineering, 104 S. Wright St., Associate Fellow, AIAA
†Scientist, Engineering Research Corporation, Member AIAA
‡Scientist, Air Force Research Laboratory, Member AIAA

Distribution Statement: Approved for public release; distribution unlimited.

the Herriott Cell can be used to measure over a volume or single point and so can be used for various testing techniques.

The Herriott Cell has been used for a variety of functions since it's inception by D. Herriott for use as a laser resonator[1]. J. Altmann et al[2] first proposed it's use in gaseous absorption measurements and it has been used extensively for that purpose. In addition, it has also been used for measurements of high reflectivity[3], as an optical delay line[3], and to produce a sequence of variable pulse separation light pulses[4]. The advantages of multiple passes in an interferometer are known, but to the best of our knowledge, the Herriott Cell has never been used in an interferometric capacity due to the uncertainty of phase front integrity over a large number of reflections on a curved surface.

The addition of a Herriott Cell to a standard interferometer has several applications to PPT research. It allows determination of electron and neutral densities during and after the pulse. Resolution of the instrument increases linearly with the number of passes. The Herriott cell also gives the ability to manipulate the beam distribution within the plasma. These capabilities allow a number of practical scientific applications. The possibility of mapping the ablation process as a function of distance from the fuel wall showing the transition from neutral to plasma and back could enable a significant increase in understanding of the ablation physics involved. The capability of making diagnostic exit plane measurements for PPTs was previously unachievable with the standard interferometric setup. Finally, the measurements from this interferometer can be used to enable spacecraft contamination modeling for flights using PPTs.

Herriott Cell Theory

A Herriott Cell consists of 2 concave mirrors facing each other in which laser light can be reflected a large number of times. Often one of the mirrors has an off-axis admission aperture that allows entrance of the beam within the diameter of the mirrors themselves. Typically, the beam enters the cell through this aperture, reflects a number of times, and leaves the cell. The number of reflections is determined by the entrance conditions consisting of mirror separation, and entrance angles. The two mirrors facing each other can be adjusted in separation distance to increase the number of passes between them. In the original configuration, the beam enters the cell at an angle both vertically and horizontally and the reflection points produce an ellipse on the surface of each mirror. This configuration is 3-dimensional, but by eliminating the horizontal entrance angle the passes can be confined to a single vertical plane ideal for measuring properties at the exit plane of rocket nozzles. Each bounce location in the single plane configuration is described by Altmann[3] as

$$x_n = x_O \cos n\theta + \sqrt{\frac{d}{4f-d}}\,(x_O + 2fx'_O)\sin n\theta \qquad (1)$$

Where n is the number of passes, d is separation distance, f is the focal length of the mirrors, x_o and x'_o are the entrance location and slope, and

$$\cos\theta = 1 - \left(\frac{d}{2f}\right) \qquad (2)$$

In addition, such parameters as mirror tilt angle and entrance hole size also affect the ability of the mirrors to operate in an interferometric setup.

In this case, a PPT exhaust is exposed to multiple laser passes for the purpose of measuring the change in index of refraction. The Herriott Cell must be designed to accommodate the maximum number of passes with the obvious restriction of keeping all of them within the plasma exhaust to be measured. To this end, two separate ray-tracing codes were employed. For the initial cell design, code was written at the University of Illinois at Urbana-Champaign varying input parameters including mirror diameter, entrance angles, aperture location and size, mirror reflectivity, and mirror separation. Coupling the code output with the constraint that the mirror separation must be between the focal length and twice the focal length[5] of the two mirrors allowed a trade study that determined the initial design of the mirrors for the cell. The reason for this requirement stems from the fact that between the mirrors there is periodic focusing for multiple reflections. Separation distances outside this requirement don't allow the possibility of attaining an acceptable exit beam diameter without external focusing optics.

After the mirrors were designed and fabricated, computer testing was done on Beam3 software for the purpose of determining feasible testing geometries. The priority was to find a plane measurement mode that would cover the exit plane of the nozzle of a typical PPT. Using the Beam3 code, a retro-reflection mode was discovered that allowed multiple pass numbers to increase with increasing separation and small to no variance in exit properties from the cell. This was one of the few geometries that allowed parallel or convergent exit beams from the cell. Figure 1 shows 6 passes in the cell

* Figs 1-4, & 9 do not have labels on the axes.

illustrated from Beam3 code. In this picture, the laser is entering from a 5 mm hole located in the upper half of the mirror on the left.

The laser reflects back on itself in this mode and by increasing the separation slightly, increasing numbers of passes can be achieved including 10, 14, 18, and 22 passes. Figure 2 and Figure 3 show 14 and 18 pass setups respectively. This retro-reflecting mode is achieved by sending the beam into the cell at 0° entrance angle both horizontally and vertically. Slight errors in entrance angle can be accommodated by adjusting the mirror tilt small amounts. For this experiment, up to 18 passes were used, but in a practical sense, depending on the mirror diameter and the location of the entrance hole the number of passes is only limited by the reflectivity of the mirrors. Output light from the cell must be adequate to make interferometric measurements. This dictates the required reflectivity for the desired number of passes.

There was considerable interest in obtaining a point measurement technique that involved focussing the beams at the center of the cell for the purpose of future use in micro-propulsion diagnostics. This would allow convergence of all the beams at a single point, an ideal setup for measuring microplasmas. The benefits of this configuration include the possibility of providing a diagnostic for micro-PPTs. Currently no diagnostics exist for this class of thrusters because of their small size and minute impulse bit. The point measurement technique has been demonstrated in the laboratory and modeled with Beam3, but no data has been taken with it to date. Figure 4 shows the Beam3 model of the point measurement geometry. The beam in Figure 4 is entering the cell from the top left this time, not through the aperture but over the side of the mirror. In addition, a lens is required to focus the incoming beam at the center of the cell equidistant from both mirrors, which are separated by a distance 2R, where R is the radius of curvature of the mirrors. This configuration is much harder to construct in a laboratory setup, requiring focussing both into and out of the Herriott cell. When the geometry is achieved a single point of convergence for all beams is not truly achieved. There are actually 2 points of convergence very close to each other. Some control over their separation can be exerted modifying entrance angle and mirror tilt, but total convergence has not been demonstrated. Raytracing modeling shows that single point convergence may not be possible. This configuration can then be used experimentally in two possible modes. The first mode fires the microthruster horizontally across both convergence points causing a loss in spatial resolution of the plasma. The spatial resolution can be maintained using the second mode at a cost in instrument resolution. By firing the microthruster vertically through only one of the convergence points, a two-fold loss in instrument resolution is suffered while the spatial resolution is maintained.

Interferometry

The interferometer is sensitive to several phenomena involved in the thruster operation. The phase change in the interferometer scene beam at the detector can be written as

$$\phi(t) = \phi_e(t) + \phi_n(t) + \phi_{PL}(t) \qquad (3)$$

where the first term represents phase change due to the plasma electron density, the second term neutral density, and the third term physical changes in the path length difference between the two beams. According to Spanjers et al[6], the phase shift due to the electron and neutral densities can be written (MKS-radians)

$$\phi_e(t) = 2.8 \times 10^{-15} \lambda \int n_e dl \qquad (4)$$

$$\phi_n(t) = \frac{3.9 \times 10^{-29}}{\lambda} \int n_n dl \qquad (5)$$

where ~~lambda~~ λ is the laser wavelength, n is the density, and the integral is performed over the path length through the probed region. The interferometer measures a line-averaged density, and requires suppositions concerning scale lengths and symmetry to reduce the measurement to a local density. The final term in equation (3) is for changes in the path length which are dominated by vibrations physically moving optic components and air currents affecting local density and temperature gradients. This can be written as

$$\phi_{PL}(t) = \frac{2\pi\Delta l}{\lambda} \qquad (6)$$

The Δl in the phase change for the path length difference represents the effective increase in optical path length for all of the environmental influences (vibration, air density, air temperature, and gradients). The dominating effect here is the vibrational differences between the optics table where the laser and detection equipment are located and the in tank optics table supporting the Herriott cell.

To resolve both electron and neutral densities, two separate laser frequencies are required as well as significant vibrational isolation. For this experiment, a single frequency is used. The data

reduction scheme involves separating the PPT breakdown into 2 domains dependent on the characteristics of the plasma at certain times. From time t_o = 0 μs until after the PPT current has died (after 20 μs for PPT-4) the assumption is made that the bulk of the phase shift is due to electron effects on the index of refraction. Due to the fact that comparable amounts of neutrals have a negligible effect on the index of refraction, the assumption is made that during the current discharge only electron density is being measured. During this phase, the contribution from physical path length changes is small due to the inherently low frequency of mechanical motion. After the discharge has died and there is no source of electrons or energy input (generally after t>20 μs) the assumption is made that there is no contribution to changes in the index of refraction from electron density. At this point the major contributors become neutral density and physical path length changes. Two frequencies can not be used to separate these two sources of phase shift since both have the same dependence on wavelength. In this case, the Herriott cell is especially valuable in increasing the sensitivity of the diagnostic to long-time-scale neutral density since the phase change due to neutral density increases linearly with number of Herriott cell passes. The Herriott cell mirrors are rigidly fixed on an optic rail, and are not exposed to room air currents. Thus, it is expected (and shown true experimentally) that the Herriott cell mirrors are not the dominant source of changes to the optical path length. The optic path between the optic table and the vacuum chamber always dominates. The phase change due to variations in the optic path length does not increase significantly with increased number of passes within the Herriott cell. This is shown in more detail below. Therefore, the accuracy of the neutral density measurement admidst environmental changes in the optic path length, almost linearly increases with Herriott cell passes. Having two measurements of the phase change (via two laser wavelengths) serves to reduce the random measurement uncertainty but has no effect on the systematic uncertainty.

Phase Front Quality

The main technical challenge to using the Herriott Cell for interferometric measurements is the ability to maintain a coherent phase front throughout the large number of reflections in the cell. The phase front is systematically distorted by imperfections in the optical surfaces from which it reflects. The high number of surface reflections will greatly decrease both the scene beam intensity and the quality of the phase front. Decreased intensity can be somewhat avoided by attenuating the intensity of the reference beam, or by adjusting the Bragg cell to increase the initial intensity of the scene beam. In practice, adding attenuation to the reference beam increases phase-front distortion, and adjusting the Bragg cell is limited to a small range in intensity variation. In addition, quantitative measurements of the beam intensity are hampered by the very large beam diameters at the detector. These result from laser divergence over the long path lengths required with the Herriott cell.

The quality of the phase front is decreased during every interaction with an optical element. Even with high surface-quality mirrors in the Herriott cell, as the number of reflections is increased the phase-front will eventually be distorted by full wavelengths across the beam diameter.

These effects can be examined analytically. At the detector, the electric field for the scene and reference beams can be written as

$$E_{scene} = E_s e^{i(w_A t + \phi(t) + \gamma(x,y))} \quad (7)$$

$$E_{reference} = E_R e^{i(w + w_A)t} \quad (8)$$

where w is the laser frequency, w_A is the acoustic frequency of the Bragg cell, Φ is the phase shift due to plasma and neutral density, and $\gamma(x,y)$ represents a phase distortion across the beam diameter. The total electric field at the detector is the sum of these components. The output voltage of the detector is proportional to the intensity, which can be calculated from

$$V \propto I = \frac{1}{2} EE^* \quad (9)$$

After some algebraic manipulation this reduces to

$$V \propto E_S^2 + E_R^2 + 2E_S E_R \cos(w_A t - \phi(t) - \gamma(x,y)) \quad (10)$$

For $E_R = E_S$ and perfect phase front (~~gamma~~=0), this reduces to the familiar expression

$$V \propto 1 + \cos(w_A t + \phi(t)) \quad (11)$$

Note that the phase front distortion can be greatly minimized at the expense of intensity. It is standard operating procedure for the normal interferometer (no Herriott cell) to use a beam up to 5 mm in diameter that is detected with a 0.5 mm square photodetector. No focussing is used to direct the full beam intensity

onto the detector. Instead, a small portion of the total beam is sampled. This has the predominant effect of increasing the spatial resolution from the diameter of the beam (5 mm) to the size of the photodetector active area (0.5 mm). Not focusing also reduces phase-front distortion, since the distortion has to occur over a scale length that is reduced by a factor of 10. For the interferometer with Herriott cell, the multiple reflections reduce the beam intensity, and the spatial resolution will be limited by the beam pattern within the cell. Therefore focusing may be used without significantly decreasing the quality of the measurement. Multiple reflections also increase the likelihood that phase-front distortions could occur over the scale length of the photodetector active area.

Figure 5 shows Eqn. (10) plotted for several relative intensities. As expected from Eqn. (11), the "50-50" curve (equal intensity) shows a simple 40 MHz oscillation. As the intensity imbalance is increased, the 40 MHz signal remains however its relative magnitude decreases. The signal also obtains a DC offset. This is equivalent to the loss of fringe contrast that occurs in the similar situation in 2-dimensional interferometers (without heterodyning). Band-pass filters at the input of the demodulation circuit will eliminate the DC offset leaving the 40 MHz signal with no phase distortion, albeit with a lower intensity. The reduced intensity will decrease signal-to-noise increasing random measurement uncertainty, but not introducing a more serious systematic uncertainty.

The effect of phase-front distortion is examined using Eqn. (10) and assuming that the two beam intensities are equal. Functional forms for the gamma term are input, and the resultant voltage is calculated by integrating over the spatial extent of the recombined beam. A simple case of this analysis is illustrated in Figure 6 where the 40 MHz output waveform is calculated for various levels of phase-front distortion. The distortion here is assumed to be linear and only occur in one direction. Furthermore, the local intensities are integrated over a square cross-section indicative of the square active area of the photodetector. More detailed analysis (although still somewhat preliminary) shows similar results for cases where the phase distortion corresponds to that expected from reflection from a curved surface, and for the case of a circular cross section (appropriate when focusing is used). As the magnitude of the phase-front distortion increases, the intensity decreases, although the 40 MHz frequency remains. For 360-degree linear distortion, the 40 MHz signal disappears as expected. For distortion greater than a full wavelength, the 40 MHz signal reappears but with significant loss of intensity. Therefore significant phase-front distortion can be tolerated and still retain the 40 MHz acousto-optic frequency in the recombined beams. For curved phase fronts, similar effects are observed except that, (1) the 40 MHz signal can shift in phase as the phase-front distortion increases, and (2) at 360-degree average phase distortion, the 40 MHz signal may remain depending on the functional form assumed for the curvature.

The more critical issue is whether the phase-front distortion effects the apparent phase change that occurs when the plasma is introduced. This is examined in Figure 7 where two signals, one with no distortion and one with a distortion of 135 degrees, are each assumed to have a 60-degree plasma phase shift. Although the signal intensity is reduced, in the case with significant phase-front distortion the full 60-degree plasma shift is observed in the 40 MHz waveform at the detector. This indicates, for the linear distortion case, that the amount of phase shift caused by the plasma density is not changed through the process of integrating the intensity over the laser beam diameter of varying phases. Linear phase distortions do not cause systematic errors in the measurement of the plasma density. Analysis with curved phase fronts shows a similar conclusion of no systematic errors in the measurement.

Experimental Apparatus

The PPT used for these measurements was the UIUC PPT-4, which is a co-axial, electrothermal PPT. The exit plane of the thruster is 4.44 cm in diameter. Fuel bars are side fed into a high pressure chamber and the exhaust is expanded out a boron nitride nozzle. The PPT performance was measured by Bushman to have 30 μN-s/J and 755 s I_{sp}[7]. The PPT was supported above an optics table in the tank and hung between the mirrors of the Herriott Cell. A small B-dot probe was placed between the capacitor terminals to trigger the scope used to obtain the firing data. Figure 8 shows the UIUC PPT-4 looking down the nozzle. The laser for the interferometer passed directly across the exit plane almost touching the brass front electrode. The PPT was fired at 20 J for each data point taken using four 2-μF capacitors in parallel for a total of 8 μF. Figure 9 shows the location of the PPT-4 exit plane within the beam spread provided by the 18 pass configuration. Figure 10 shows a schematic of PPT-4. The interferometer laser passes directly in front of the cathode.

The interferometer is laid out on a single optics table with the exception of the Herriott Cell that is stationed within the vacuum chamber. Figure 11 shows the interferometer layout that was used for this experiment. Only the 488-nm wavelength laser has been used to date, but transition to a 2-color

system can be readily accomplished. The infrared laser will be added at a later date to allow separation of neutral and electron densities.

The beam exits the laser, passes through a 488 nm line filter, and a 40 MHz oscillation is acousto-optically introduced through a Bragg Cell. This splits the beam into the zeroth and first order beams which are taken as scene and reference beams respectively. The scene beam is then directed into the chamber and the Herriott Cell. Within the cell the scene beam reflects a pre-determined number of times and exits at a slight angle from the input beam. The output is picked off and recombined with the reference beam in a wavelength-tuned beamsplitter. From there the recombined beam goes into the photodetector. It's important to note here that the scene and reference beams must have the same path length from the Bragg Cell to the recombining beamsplitter within a small percentage of the coherence length of the laser. For the Ar-ion laser used here, the coherence length was 10 cm, so the path lengths needed to be matched to within less than 1 mm. This was achieved using a micrometer mirror mount on an optical rail for the reference beam. The beam then entered and exited at a very small angle from the normal to the mirror surface. Rough tuning was done moving the mount manually and precise tuning then performed with the micrometer.

Following the recombination of the beams and measurement at the detector, the signal from the detector was then demodulated using a mini-circuit consisting of 2 mixers, a power splitter, and a 90° phase shifter shown in Figure 12. The output of this circuit is the cosine and sine functions of the unreduced phase shift. Reduction of the phase shift involves performing numerical quadrature on these signals through use of a Fortran code written at AFRL.

Herriott Cell Design and Beam Shields

The cell design included mirrors with a 2-inch diameter and a radius of curvature (r_c) of 8 inches. Since $r_c = 2f$, the focal length was 4 inches for each mirror. On one mirror there is a 5-mm diameter admission aperture that is located 11 mm radially off the mirror axis. Smaller entrance holes were tested, but they reduced the intensity of the output light significantly. The location of the entrance hole is a constraint on the vertical spatial coverage that can be achieved with the Herriott Cell. Typically, the beam spread is contained within twice the off axis diameter of the entrance hole. This can be stretched somewhat by using mirror tilting, but the effects are limited.

The mirrors used were $\lambda/10$ surface flatness and coated with an UV enhanced aluminum coating. This coating is used because it has greater than 90% reflectivity from 250-600 nm. This was ideal for use of a 488-nm Argon ion laser and allowed the possibility of using a 351-nm UV laser due to greater neutral sensitivity at lower wavelengths. For a 633-nm HeNe, reflectivity is about 90% and for an IR laser at 1100 nm, reflectivity goes up to 92%. These colors can be used for greater electron sensitivity in a two-color interferometer. Even at 90% reflectivity, only 15% of the light incident to the cell exits at 18 passes. This number also neglects aggravating effects from optics external to the cell. It is for this reason that more than 18 passes were not attempted. While the cell is capable of providing the required geometry, a higher power laser or more reflective mirrors are required to make use of large numbers of passes.

The physical constraint of $f \leq d \leq 2f$ limits the separation distance[5] of the mirrors to between 4 to 8 inches for the retro-reflecting mode. This was initially thought to be adequate to allow for the nozzle of UIUC PPT-4 or the parallel plates of a LES 8/9 type PPT, but it was later determined that a larger mirror diameter (~3-4 in.) along with a larger radius of curvature (~8 in.) is optimal. The necessity of a larger mirror diameter becomes apparent when attempting to measure a larger vertical area. In this case, the off axis location of the entrance hole becomes critical. For a 50.8-mm diameter mirror, placing the 5-mm diameter entrance hole at 21 mm off center will not provide a reflective beam pattern. The reason for this is that spot pattern on the mirror opposite the beam entrance is slightly larger than the entrance hole distance from the mirror axis. In addition, a larger radius of curvature is of interest because it allows a greater mirror separation for the same number of passes. At first glance, this would appear to be counterproductive owing to greater beam dispersion over an already extensive total path length. Unfortunately, plasma impact on the mirrors aggravates mechanical vibrations already present increasing the amplitudes by significant fractions of a phase shift. This has the effect of masking late neutral densities and precludes measuring the neutral density return to zero. Figure 13 shows this effect on a long timeframe compared to the natural room vibrations. Because of these induced vibrations, data taken beyond 300 us into the pulse was considered suspect and unusable. This makes it difficult if not impossible to witness the return of measured neutral density to zero.

In the original design concerns about plasma mirror interactions were geared toward the buildup of Teflon on the mirrors and the effects the coating would have on reflectivity. Beam shields were designed to minimize the exposed surface area by

providing a metal cover over the mirror with a corridor allowing vertical reflections. Figure 14 shows the Herriott cell with beam shields in place. The beam shields failed to damp the mechanical vibrations induced by the plasma impact, and otherwise were innocuous to cell operation.

Experimental Results

Density vs. Number of Passes

Tests were conducted using PPT-4 under the same testing conditions for various numbers of passes. From 2 to 18 passes were tested to compare the measured densities and determine statistical and systematic uncetainties. The 2-pass system was simply a flat mirror returning the beam through the plasma typical of a standard interferometric setup. 6, 14 and 18 pass tests were performed for comparison to the standard interferometer setup. In comparing data from these four methods detailed attention must be paid to the uncertainty analysis. In the standard interferometric setup, the largest source of uncertainty is between the vacuum chamber and the optics table with the laser and photodetectors. When an additional mirror is added in the tank, some increase in vibrational uncertainty is expected. For the Herriott Cell to be effective there must be no noticeable increase in vibrational noise for additional laser passes between the mirrors. In this case, the vibrational noise level remains constant while the resolution of the instrument is increased proportional to the number of passes. In addition to that requirement, different numbers of passes should return the same electron and neutral densities within the shot-to-shot variation of the thruster being tested. This indicates that there is no systematic error introduced by the Herriott Cell. Due to diminishing returns in laser intensity, more than 18 passes were not attempted. Figure 15 shows the increase in phase shift for increasing number of passes in the cell. The 4 shots were taken at random from the total number of shots taken on PPT-4. The trace seen is the angular data for each shot shown. For the data in all cases, early in the pulse where peak electron density is measured, the vibrational uncertainty is ±0.5°. At 200 μs into the pulse, the vibrational uncertainty is approximately ±19° for the cases shown. For the case of 2 passes, the uncertainty is ±10°. Figure 16 shows the changes in vibrational uncertainty for 2-18 passes. From 2 – 6 passes, there is an increase in the vibrational uncertainty that corresponds to the addition of the extra optic for the Herriott Cell. Note that varying from 6-18 passes shows no noticeable increase in vibrational uncertainty. Thus, going from a 2 to 18 pass setup decreases the resolution by 2x but increases by 9x. In addition, the 19° uncertainty measured for the Herriott Cell system is only a consequence of the vibration suppression measures taken and can vary from system to system. In favorable conditions, the vibrational uncertainty at long timeframes can become very low.

Uncertainty Terms

The increase in phase shift measured for a given thruster is linear with an increase in passes within the shot-to-shot variation of the thruster itself. In the case of a PPT, the uncertainty in density consists of 2 terms.

$$\Delta n = \sqrt{\Delta n_{vibs}^2 + \Delta n_{PPT}^2} \qquad (12)$$

Where Δn_{vibs} is the uncertainty due to vibrations and Δn_{PPT} is the shot-to-shot variation of the PPT in question. The vibrational uncertainty is quantified as

$$\Delta n_{vibs} = C\frac{\Delta\Phi}{N} \qquad (13)$$

Where N is the number of passes in through the plasma. For large numbers of passes, the effect on vibrational uncertainty is advantageous at long timeframes. The number of passes has no effect on the Δn_{PPT} term in equation (12). This term is dependent on the firing repeatability of the plasma source being measured. Although there is no direct dependence on phase shift for the statistical term, at late times it is possible for the vibrational uncertainty to overwhelm the statistical variation observed. Figure 17 shows a single set of data for 18 passes with local vibrational uncertainty measurements shown with the firing data. The vibration traces are the average and positive and negative standard deviations for 20 shots taken just prior to 20 shots of firing data. In this case special attention is paid to the timeframe between 20 and 160 ms. During this timeframe, the average firing data from the 20 shots recorded lies outside the negative standard deviation for the vibration measurements. This is a definite indication of neutral density measurement with 18 passes in the Herriott cell. The firing deviation for the electron density peaks is ±50° while the vibrational deviations are only ±0.5°. When this data is compared with the case of 2 pass data for the same parameters, the advantage is apparent. Figure 17 shows comparable 2 pass data for 20 vibration shots and 20 firing shots. While the measurement is more than adequate for the electron density, no discernible neutrals are evident. Without the increase in resolution from the Herriott cells, the standard

interferometric setup fails to produce a definitive neutral measurement.

For Pulsed Plasma Thrusters, the measured densities are variable within a statistically determined range. For this reason, both electron and neutral densities are averaged over a large number of shots with statistical error bars demonstrating the range of the performance variation from shot to shot. The standard deviation at any specific time over large sampling of firings determines the uncertainty Δn_{PPT}. Depending on what time during the pulse is of interest, either of these uncertainties can be dominant. Figure 19 shows the electron density at time 4 μs after the pulse. Measured electron density showed peak density at 4 μs to be $5.0*10^{15} \pm 1.1*10^{15}$ cm^{-3}. The vibrational uncertainty bars here are smaller than the data point used to represent each point because they correspond to ±0.5° early in the pulse. The dominant uncertainty at this point is clearly the shot-to-shot variation of the thruster itself. For varying numbers of passes, it is apparent that the measured densities fall within the statistical uncertainty bars of each other. This experimentally verifies the above analytical conclusion that there is no systematic error induced by the Herriott Cell.

The case of the neutral densities is slightly different because these are naturally occurring later in the pulse. Vibrational uncertainty can be just as large if not larger than the statistical differences in thruster firings in this regime. Figure 20 shows the neutral densities at 200 us into the pulse. This shows the neutral density at 200 μs to be no more than $1*10^{16}$ cm^{-3}. Here the benefits of many passes are obvious. Both the vibrational and total uncertainties are decreasing as a function of the number of passes in the Herriott Cell. At this point the vibrational uncertainty dominates allowing total uncertainty to decrease significantly as a function of passes. The total uncertainty can be characterized at any point in the discharge by the standard deviation over large numbers of shots in similar vibrational conditions. It is for this reason that each test consists of at least 20 data shots for vibrations and 20 PPT firings for density data. Since vibrational uncertainty can be affected by different occurrences in the laboratory, each test requires it's own uncertainty calibration.

Conclusions

The Herriott cell can be a valuable addition to interferometry for use in determining neutral densities and measurements of microplasmas. Experimental and analytical analysis demonstrates the integrity of the phase front is retained to a quality high enough for interferometric purposes. Comparison of a standard interferometric setup with varying numbers of passes in the Herriott cell was performed. Over varying number of passes in the cell the electron and neutral densities measured consistently fell within the statistical shot-to-shot variation of the thruster used. At early times in the pulse, the statistical variation of the thruster itself dominates the uncertainty term. Later in the pulse physical path length changes due to external vibration sources come to dominate the uncertainty of the measurement. In this operating regime the Herriott cell becomes invaluable to the operation of the diagnostic. Use for standard PPTs is feasible at this point for plume modeling and spacecraft contamination purposes for future missions. Additionally, use for measurements of small scale plasmas generated by pulsed micro-thrusters is yet to be tested, but the required geometries have been demonstrated in the laboratory.

References

1. D. R. Herriott, H. Kogelnik, R. Kompfner, "Off Axis Paths in Spherical Mirror Interferometers," Applied Optics 3, 1964, 523.
2. J. Altmann, P. Pokrowsky, "Sulfur dioxide absorption at DF laser wavelengths," Applied Optics Vol. 19, No. 20, 1980, pp. 3449-3452.
3. D. R. Herriott, H. J. Schulte, "Folded Optical Delay Lines," Applied Optics Vol. 4, No. 8, 1965, pp. 883-889
4. J. Brochard, P. Cahuzac, "Use of multi-path optical cavities in some saturated absorption experiments. Frequency scale and optical delay line." J. Optics (Paris) Vol. 8, No. 3, 1977, pp. 207-211
5. J. Altmann, R. Baumgart, C. Weitkamp, "Two mirror multipass absorption cell," Applied Optics Vol. 20, No. 6, 1981, pp. 995-999
6. G. G. Spanjers, K. A. McFall, F. S. Gulczinski, R. A. Spores, "Investigation of Propellant Inefficiencies in a Pulsed Plasma Thruster," 32nd *AIAA/ASME/SAE/ASEE Joint Propulsion Conference and Exhibit*, AIAA paper 96-2723, Lake Buena Vista, FL, July 1998
7. S. S. Bushman, *Investigations of a Coaxial Pulsed Plasma Thruster*, University of Illinois at Urbana-Champaign, 1999

Figures

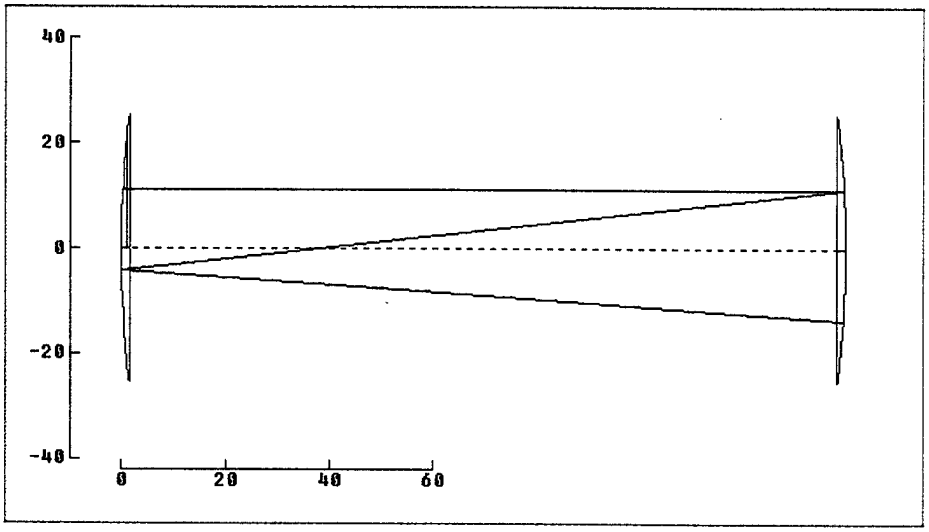

Figure 1. 6 Passes in Retro Reflecting Mode

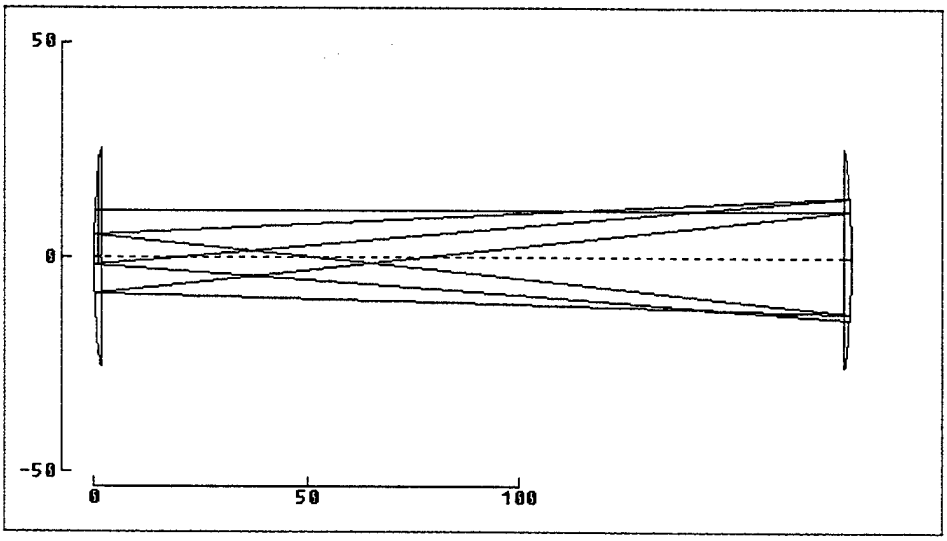

Figure 2. 14 Passes in Retro-reflecting Mode

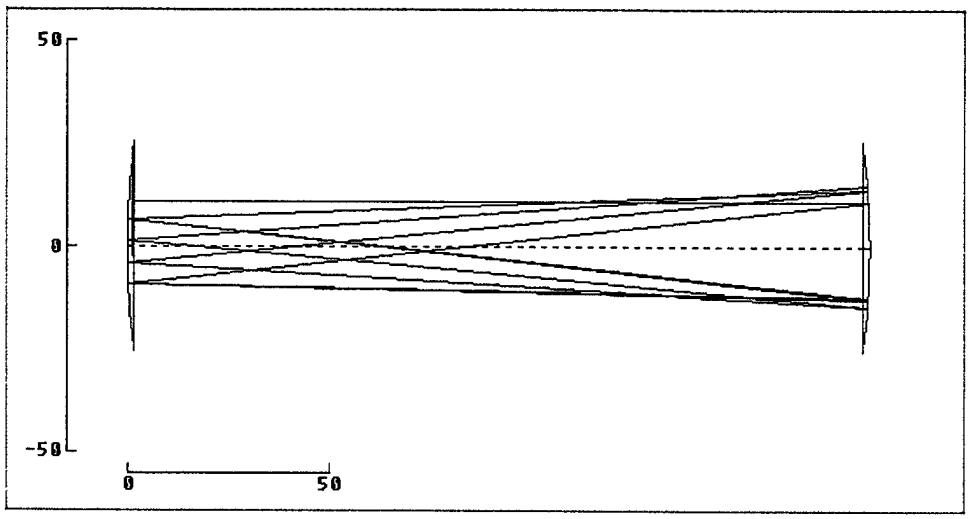

Figure 3. 18 Passes in Retro-reflecting Mode

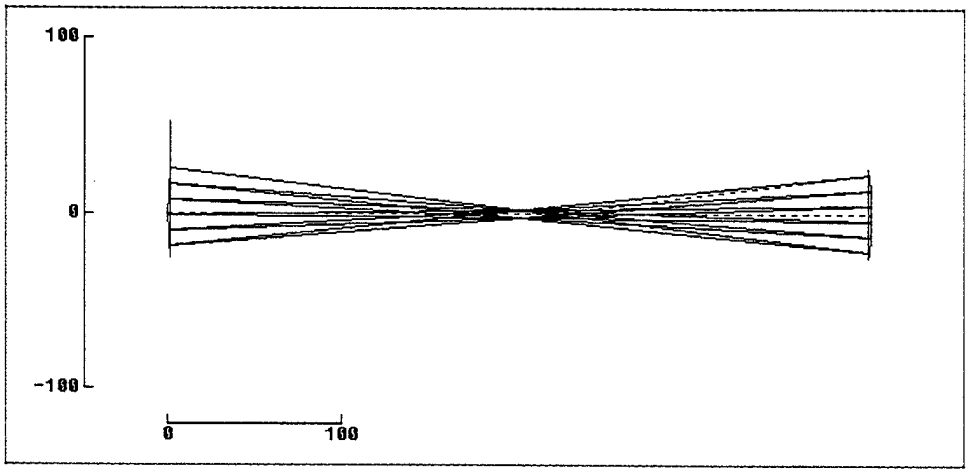

Figure 4. Point Measurement Geometry

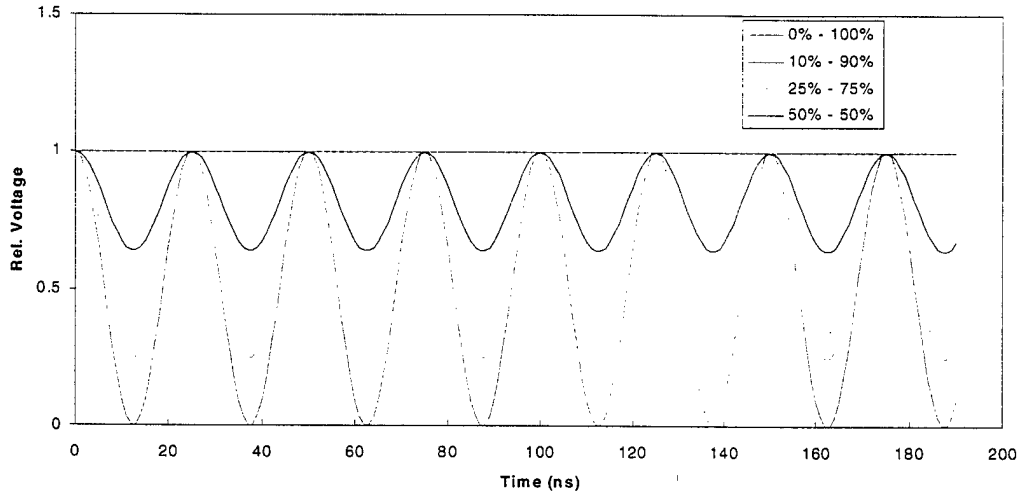

Figure 5. Effect of non-balanced intensities on the interferometer signal at the detector. Percentages in legend refer to the relative intensities of the scene and reference beams.

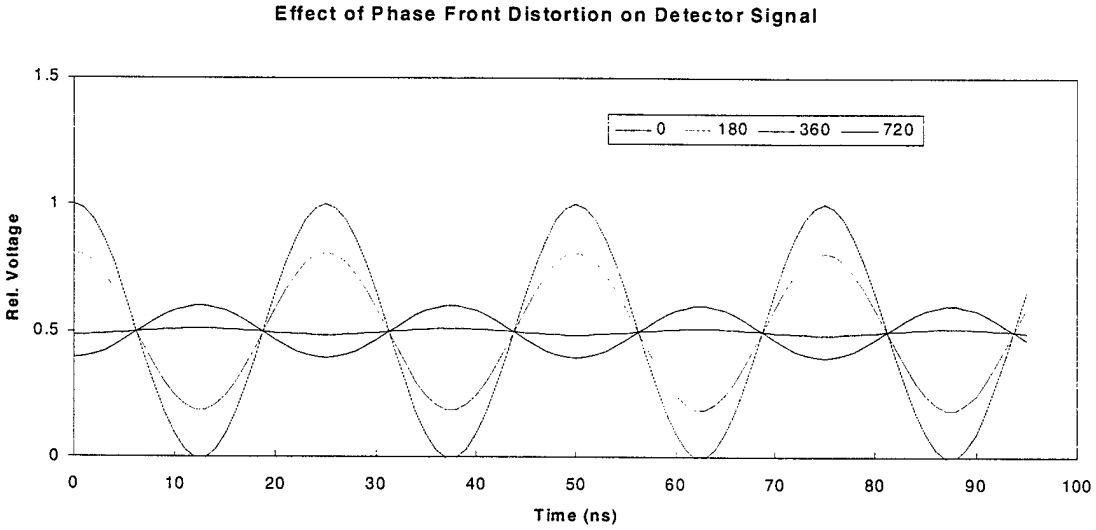

Figure 6. Detector output signal for varying magnitudes of phase-front distortion. The trace labeled "0" corresponds to zero phase distortion, "180" corresponds to ½ wavelength distortion, etc. In each case, the distortion is presumed linear in one direction across the beam diameter and the beam is presumed square.

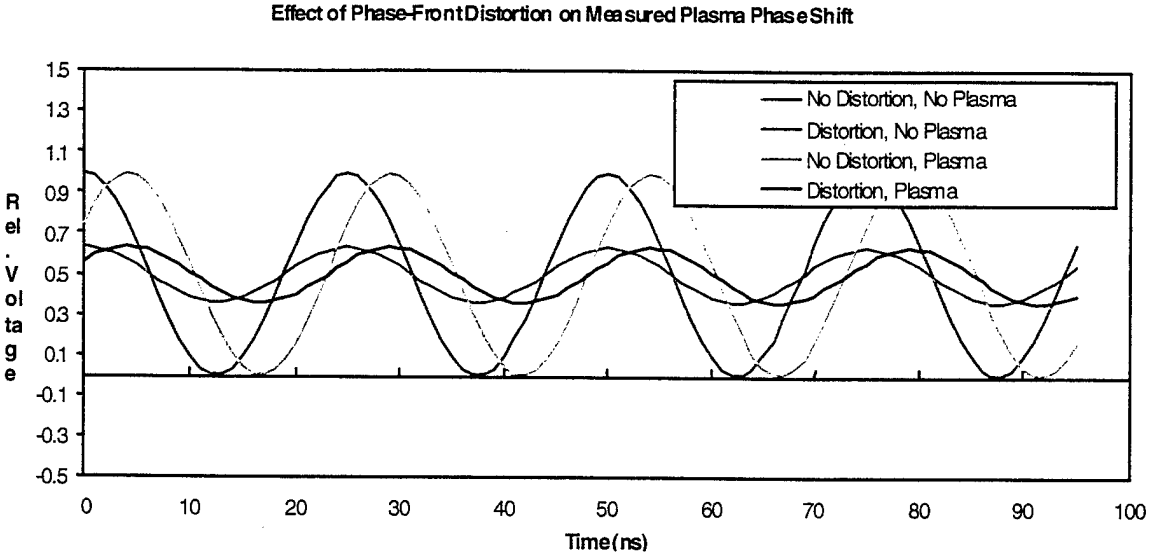

Figure 7. Effect of Phase-front distortion when a plasma-induced phase shift is present.

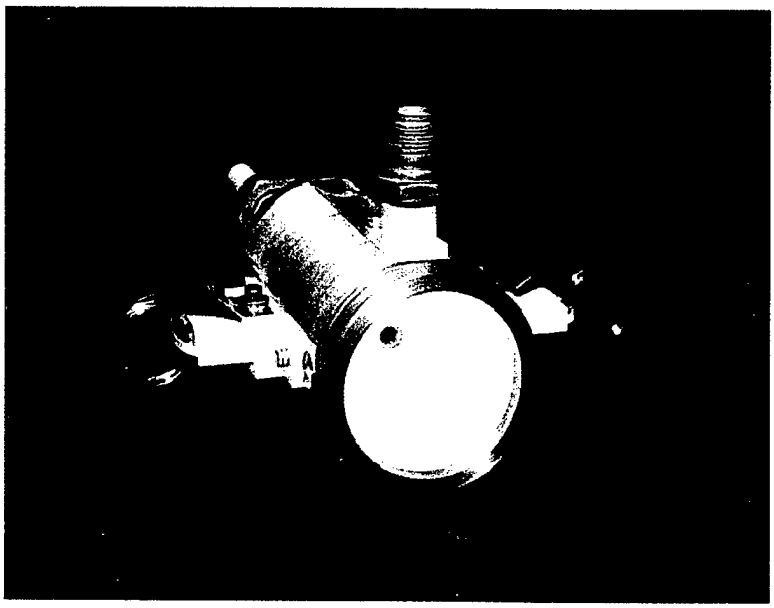

Figure 8. Frontal View of UIUC PPT-4

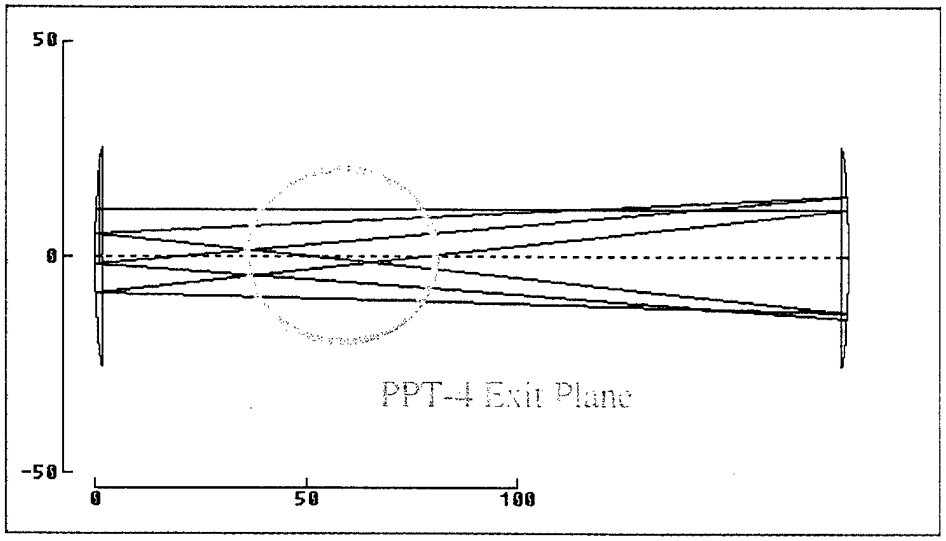

Figure 9. 18 pass configuration showing location of PPT-4 exit plane.

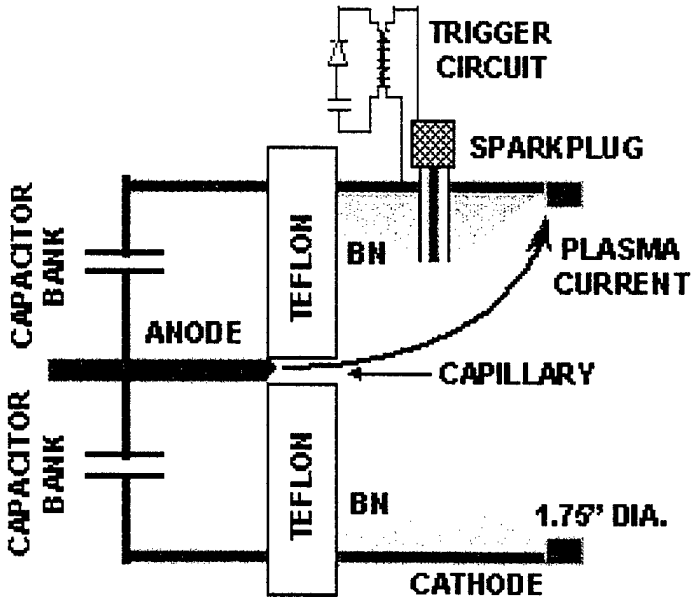

Figure 10. Schematic of PPT-4

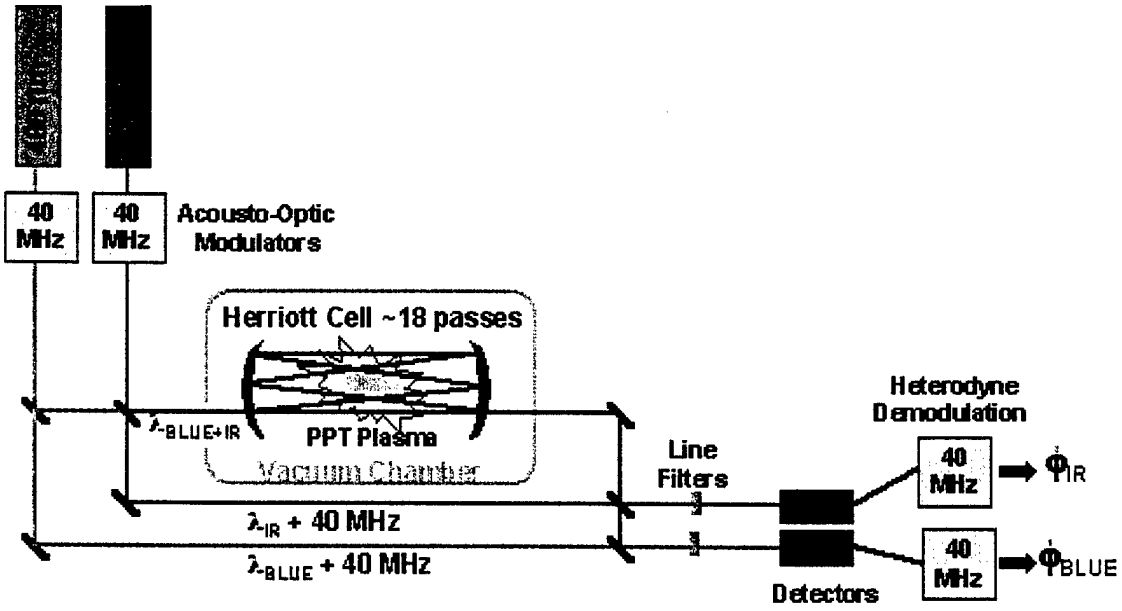

Figure 11. Interferometer layout with optional second wavelength

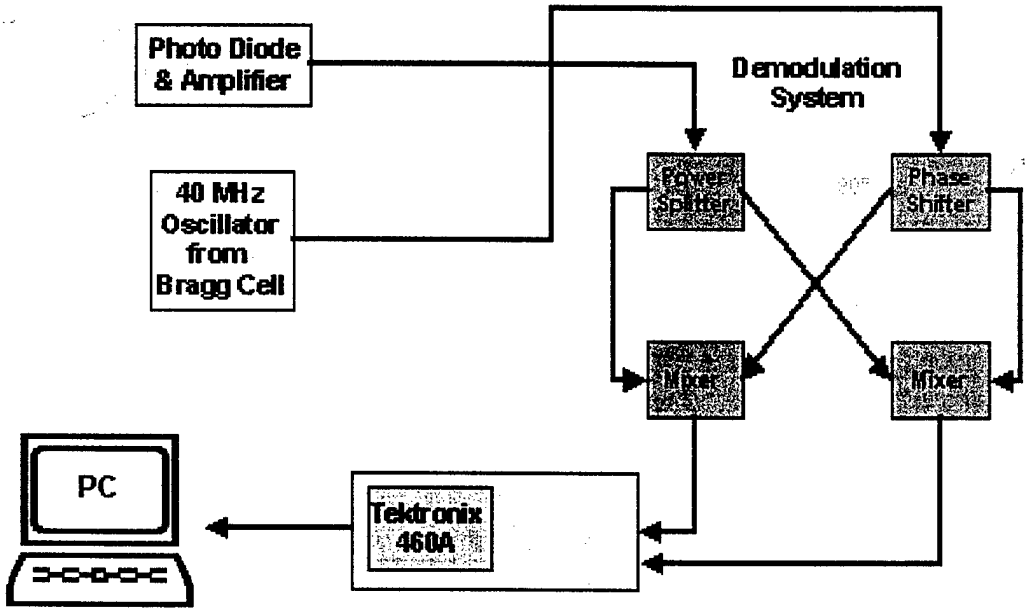

Figure 12. Post detection processing schematic

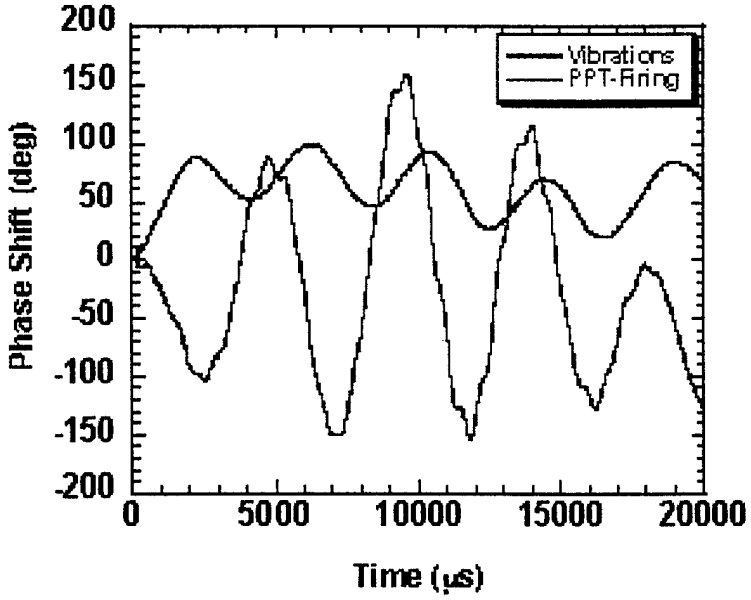

Figure 13. Plasma-mirror interactions increase room vibration amplitudes

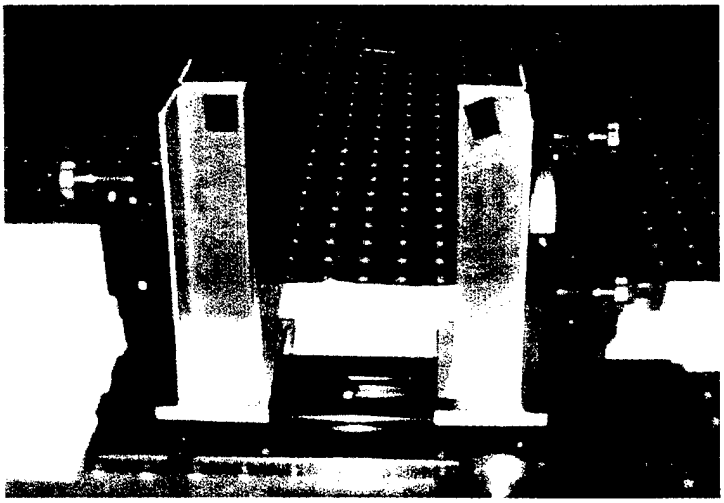

Figure 14. Herriott Cell with Beam Shields

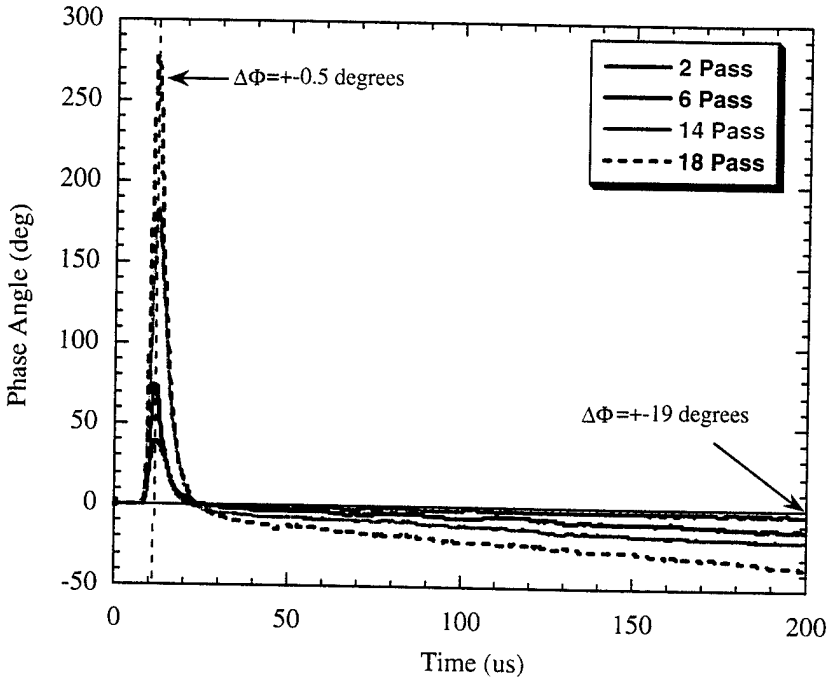

Figure 15. Four raw data shots showing increase in phase shift with passes over 200 us timeframe.

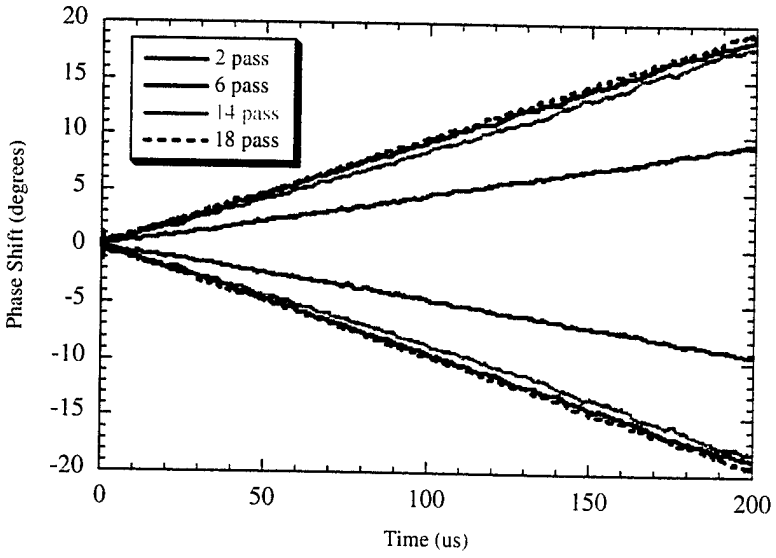

Figure 16. Comparison of vibration growth over 200 μs for 2 – 18 passes.

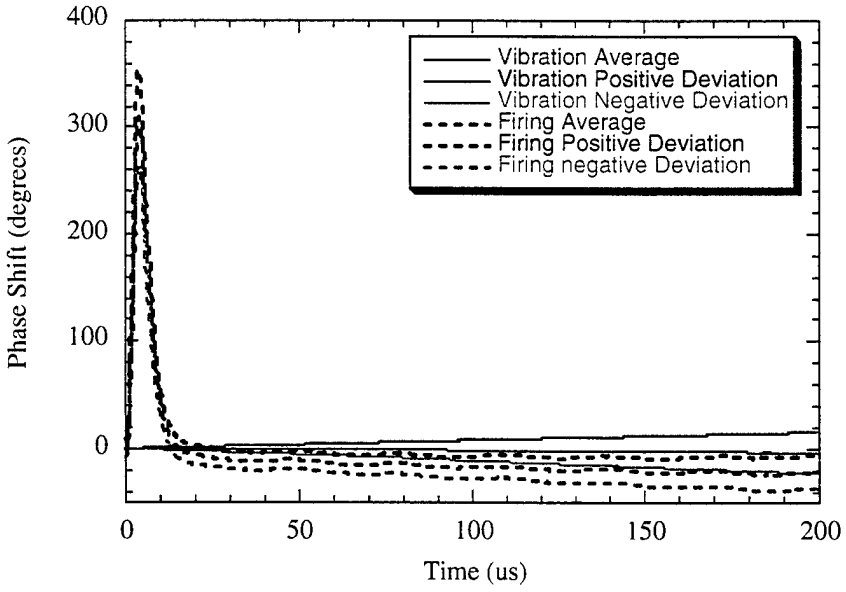

Figure 17. An 18-pass data set with vibrational uncertainty from 20 shots taken when testing.

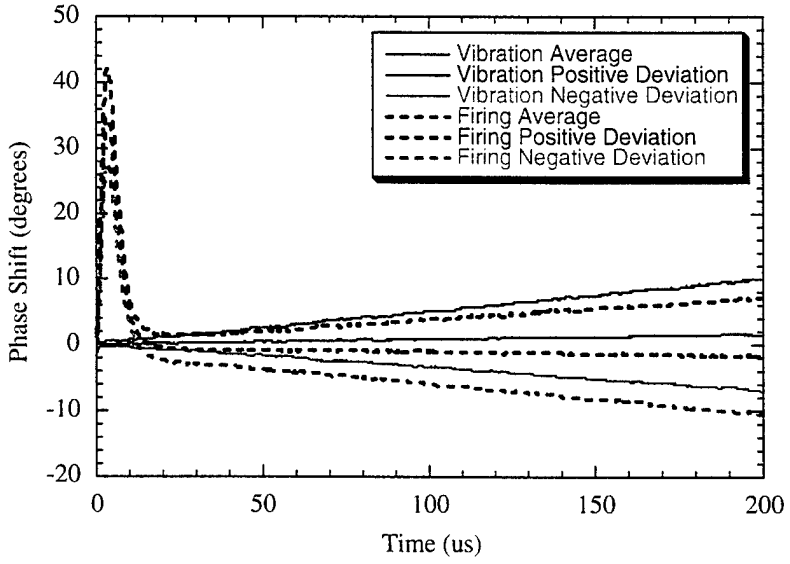

Figure 18. A 2-pass data set with vibrational uncertainty from 20 shots taken when testing.

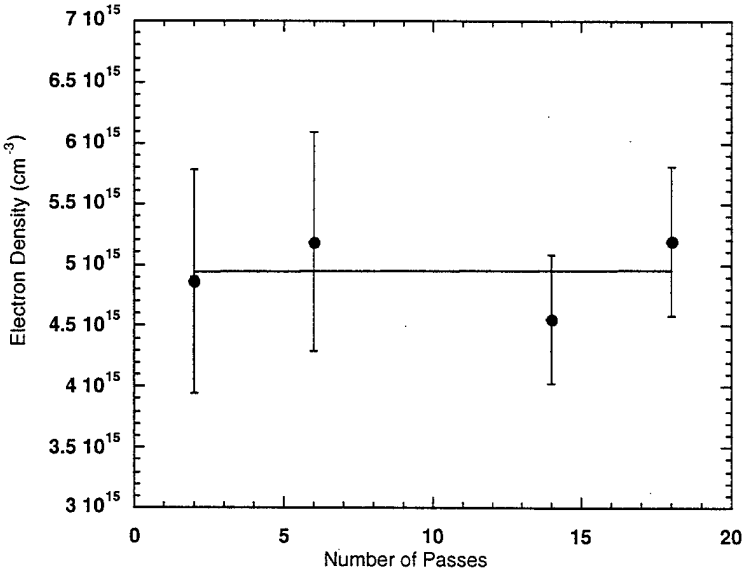

Figure 19. Electron densities at 4 us for increasing number of passes with statistical (blue) and vibrational (purple) uncertainty bars.

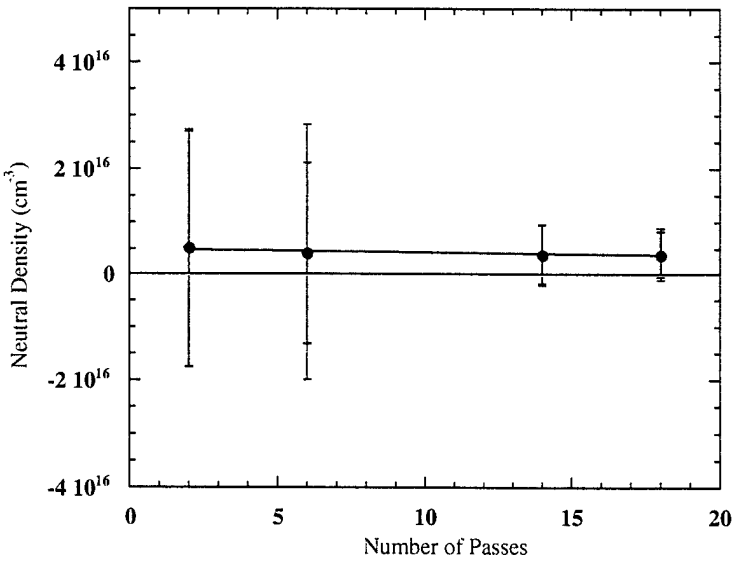

Figure 20. Neutral Densities at 200 us for increasing number of passes with statistical (blue) and vibrational (red) uncertainty bars.